

Article

# Influence of the Architecture of Soft Polymer-Functionalized Polymer Nanoparticles on Their Dynamics in Suspension

Young-Gon Kim, Waraporn Wichaita  and Héloïse Thérien-Aubin \*

Max Planck Institute for Polymer Research, Ackermannweg 10, 55131 Mainz, Germany; kimyoung@mpip-mainz.mpg.de (Y.-G.K.); waraporn.wic@gmail.com (W.W.)

\* Correspondence: therien@mpip-mainz.mpg.de

Received: 4 August 2020; Accepted: 14 August 2020; Published: 17 August 2020



**Abstract:** The behavior of nanogels in suspension can be dramatically affected by the grafting of a canopy of end-tethered polymer chains. The architecture of the interfacial layer, defined by the grafting density and length of the polymer chains, is a crucial parameter in defining the conformation and influencing the dynamics of the grafted chains. However, the influence of this architecture when the core substrate is itself soft and mobile is complex; the dynamics of the core influences the dynamics of the tethered chains, and, conversely, the dynamics of the tethered chains can influence the dynamics of the core. Here, poly(styrene) (PS) particles were functionalized with poly(methyl acrylate) (PMA) chains and swollen in a common solvent. NMR relaxation reveals that the confinement influences the mobility of the grafted chain more prominently for densely grafted short chains. The correlation time associated with the relaxation of the PMA increased by more than 20% when the grafting density increased for short chains, but for less than 10% for long chains. This phenomenon is likely due to the steric hindrance created by the close proximity to the rigid core and of the neighboring chains. More interestingly, a thick layer of a densely grafted PMA canopy efficiently increases the local mobility of the PS cores, with a reduction of the correlation time of more than 30%. These results suggest an interplay between the dynamics of the core and the dynamics of the canopy.

**Keywords:** soft nanoparticles; grafted polymer chains; grafting density; NMR; relaxation

## 1. Introduction

Nanoparticles (NP) possess a large surface area to volume ratio, and the control of the interface has a critical influence on the properties of the NP systems by tuning their interaction with their surrounding environment. Controlling the interfacial properties is critical since the incompatibility of the NPs with their surrounding media can result in the agglomeration of the NPs. The interfacial properties of the NPs can be controlled by tethering polymer chains at the interface, to improve the NPs compatibility with a solvent or a polymer matrix [1–5]. The layer of tethered polymers, whether the chains are in a brush conformation or not, forms a canopy around the core particle, and this layer of grafted chains defines the interaction between the NPs and between the NPs and their environment [6]. In such cases, the final behavior of the NPs is influenced by the chemical composition of the grafted chains, but also by their degree of polymerization ( $N$ ) and their grafting density, the number of grafted chains per unit of area ( $\sigma$ ). Variations in  $N$  and  $\sigma$  in systems where the polymer chains are tethered to hard and rigid nanoparticle core, such as silica or gold, influence the dynamics of the grafted polymer chains. And the architecture of the canopy of grafted polymer chains defines the interfacial properties of the NPs, such as particle/particles interaction or NPs/solvent interaction [6–11]. However, the behavior of systems where the core is itself soft and deformable like a nanogel has not been addressed, and the

dynamics of polymer chains grafted on the surface of soft NPs need to be thoroughly understood to improve the design of such systems [12].

The architecture of the grafted polymer system, defined by the  $\sigma$  and  $N$  of the canopy, affects the conformation [13–15] and the dynamics of the grafted chains [16]. Both of which, in turns, largely affect the macroscopic behavior of systems based on polymer-functionalized NPs, such as the mechanical properties of nanocomposites [16,17] or the rheology of colloidal suspensions [11,16,18]. In a polymer-grafted NPs system, usually, the polymer chains experience a deceleration of the relaxation in comparison to free chains as a consequence of the stretched chain conformation near the surface of nanoparticles and increased confinement generated by the proximity of adjacent chains [19] at least at the scale of the local segmental motion. On a larger scale, the increased confinement experienced by densely grafting chains usually resulted in an increase of glass transition temperature of tethered chains in comparison to the free chains ascribed to the presence of a reduced number of chain ends and smaller free volume in the grafted system [20–22].

The investigations of the behavior of polymer grafted nanoparticulate systems have mostly dealt with rigid core NPs like silica or gold. However, when soft and swollen polymer NPs are used as the substrate, the intrinsic dynamics of the polymer chains in the core also needs to be taken into account. In such swollen polymer nanoparticles, the dynamics of the chains is typically constrained and sparsely crosslinked nanogel displayed a soft interface with polymer chains having a rapid relaxation, while densely crosslinked nanogels exhibited glassy surface with constrained local mobility [23–25]. In nanocolloids resulting from the self-assembly of block copolymers, this arrested core is surrounded by a canopy of swollen and mobile polymer chains. In such a case, the polymer chains within the core experienced a soft confinement, where the dynamics is influenced by the fluctuation of the interface where the two polymer components are connected [26]. Such phenomena affect the design of soft particles for different applications, for example, theranostic systems [23,25,27]. While block copolymer micelles are an interesting point of comparison to the polymer-functionalized nanoparticles, in such systems, the effect of the density of the surface functionalization on the local dynamics cannot be addressed, since it is difficult to control the packing density.

Here, the combined effects of the  $N$  and the  $\sigma$  of the grafted canopy on the dynamics of both the core and the canopy of polymer-functionalized polymer nanoparticles were investigated using NMR relaxometry. Polystyrene (PS) NPs functionalized with a canopy of end-grafted poly(methyl acrylate) (PMA) were prepared by a combination of miniemulsion polymerization and surface-initiated polymerization, and dispersed in a common good solvent for both the core and the canopy. The  $\sigma$  was controlled and resulted in different canopies composed of either stretched polymer chains or collapsed chains (Figure 1a). The  $N$  of the grafted chains was also modified, so the contour length of the grafted PMA chains was increased from ca. 7 to 150 nm, while the radius of the swollen PS core was kept constant at ca. 100 nm. NMR relaxometry gave access to the correlation time ( $\tau_c$ ) associated with the subsegmental dynamics of the polymers [28,29]. The activation energy associated with the subsegmental dynamics of the polymer NPs in suspensions was analyzed and compared to the thermal behavior of the dried NPs.

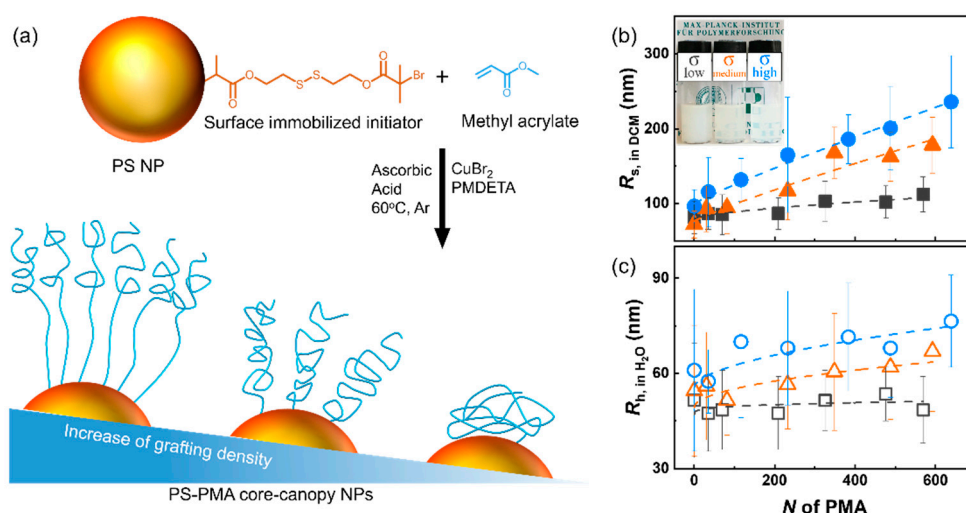


**Figure 1.** (a) Synthesis of poly(styrene) (PS)-poly(methyl acrylate) (PMA) core-canopy nanoparticles (NPs); (b) Solvodynamic radii ( $R_s$ ) and (c) hydrodynamic radii ( $R_h$ ) of PS-PMA NPs in DCM and H<sub>2</sub>O, respectively. For NPs functionalized with PMA chains with a degree of polymerization ( $N$ ) ranging from 0 to 639 units with low (0.17 chains nm<sup>-2</sup>, □), medium (0.8 chains nm<sup>-2</sup>, △) and high (2.5 chains nm<sup>-2</sup>, ○) grafting density, measured by dynamic light scattering at 25 °C. The inset photo in (b) displays the suspensions of PS-PMA<sub>49k-σ<sub>low</sub></sub>, PS-PMA<sub>51k-σ<sub>medium</sub></sub>, and PS-PMA<sub>55k-σ<sub>high</sub></sub> in DCM at a concentration of 16.67 mg mL<sup>-1</sup>.

## 2. Materials and Methods

### 2.1. Materials

The ATRP inimer (2-((2-(3-methyl-2-oxobut-3-en-1yl)xy)ethyl)disulfanyl)ethyl 2-bromo-2-methylpropanoate) was synthesized as previously reported [18,30]. Styrene (99%, Sigma-Aldrich, Darmstadt, Germany), methylacrylate (99%, Sigma-Aldrich, Darmstadt, Germany) and divinylbenzene (80%, Alfa Aesar, Ward Hill, MA, USA) were purified with a basic aluminum oxide column (Sigma-Aldrich, Darmstadt, Germany). 2,2'-azobis(2-methylbutyronitrile) (V-59, WAKO, Osaka, Japan) was recrystallized in methanol (MeOH). All other chemical reagents were used as received.

### 2.2. Synthesis of Nanoparticles Functionalized with ATRP Inimer (PS-Br NPs)

In a typical procedure, 28 mmol of styrene (St, 0.99 eq.), 287 μmol of divinylbenzene (DVB, 0.01 eq.) and 38 mmol of hexadecane (HD, 0.04 eq.) were added to a 40 mL vial and were mixed with 144 μmol of a V-59 (0.005 eq.). After 10 min of mild stirring, 24 mL of 10 mM of aqueous solution of sodium dodecyl sulfate (SDS) was added, and vigorously stirred for 15 min. The mixture was emulsified by using a probe sonicator (Branson 450 Digital Sonifier, Danbury, CT, US) equipped with a titanium solid extender tip, diameter of 1/2" for 2 min at 0 °C (20 kHz, 70% amplitude, 10 s on/2 s off). The resulting miniemulsion was transferred to a 50 mL round bottom flask and heated at 80 °C to initiate polymerization. After 2.5 h of reaction, 2 mL of SDS aqueous solution (250 mM) was added and the reaction mixture was degassed by bubbling with Ar for 10 min. Then, in order to cover PS core NPs with a thin layer of ATRP inimer (Figure 1a), a mixture of St (5.8 mmol, 0.99 eq.), DVB (58 μmol, 0.01 eq.), ATRP inimer (59–590 μmol, 0.01–0.1 eq.) and V-59 (30 μmol) was added dropwise, at a rate of 1 mL h<sup>-1</sup>. The mixture reacted overnight at 80 °C and was then filtered. The PS NPs in the aqueous suspension were purified by precipitation in 200 mL of MeOH and air-dried. To obtain impurity-free PS NPs without HD and SDS, the NPs were redispersed in 40 mL of THF, precipitated in 500 mL of MeOH three times and redispersed in THF and precipitated in hexane. Finally, the NPs were air-dried.

### 2.3. Synthesis of the End-Tethered Canopy of PMA on the Surface of the PS Core (PS-PMA NPs)

The end-tethered PMA canopy was grafted from PS core by surface-initiated ATRP (Figure 1). A solution of methyl acrylate (4.4 mmol) dissolved in 0.1 mL of DMF containing Cu(II)Br<sub>2</sub> (2000 ppm) and PMDETA (Cu(II):PMDETA = 1:10) was added into a 25 mL Schlenk tube containing a suspension of the PS-Br NPs functionalized with the ATRP initiator (50 mg) dispersed in anisole (4 mL). PDMS (0.1 mL) was added to the suspension as internal standard. The mixture was stirred and degassed with argon for 30 min. In order to initiate the polymerization, 0.5 mL of DMF containing ascorbic acid (1600 ppm) was added. This resulting suspension was further degassed with argon for 10 min, and the reaction vessel was heated at 60 °C and allowed to react. When the targeted monomer conversion was obtained, the reaction mixture was diluted with 10 mL of THF, precipitated in 100 mL of MeOH. The PS-PMA core-canopy NPs were purified three times by redispersing the NPs in 20 mL of DCM and precipitating in 100 mL of *n*-hexane. The NPs were then dried overnight under vacuum. The reaction was repeated by varying the amounts of the monomer, Cu(II)/ligand and bromoisobutyrate grafted moieties. For the free PMA chains, the appropriate molar amount of ethyl  $\alpha$ -bromoisobutyrate (Sigma-Aldrich, Darmstadt, Germany) was used as the ATRP initiator in the reaction mixture instead of PS-Br NPs.

### 2.4. Characterization

The solvodynamic radius of the NPs was determined by dynamic light scattering (DLS) measured with a Malvern Instruments Zetasizer Nano S90 (Malvern, UK) at a fixed angle of 90° ( $\lambda = 633$  nm, 15 runs, run duration of 10 s). The nanoparticles were dispersed either in DCM or in an aqueous solution of CTAC at a concentration of 0.05 mg mL<sup>-1</sup>. All the measurements were carried out at 25 °C. The  $\sigma$  was measured by inductively coupled plasma atomic emission spectrometry (ICP-AES) with an ACTIVA M spectrometer (Horiba Jobin Yvon) equipped with a Meinhardt-type nebulizer and a cyclone chamber, and processed by the software ACTIVAnalyst 5.4. The glass transition temperatures of the NPs were measured by using differential scanning calorimetry (DSC, 204F1/ASC Phönix, Netzsch, Selb, Germany) under nitrogen flow of 20 mL min<sup>-1</sup> between -80 to 200 °C at heating and cooling rates of 10 K min<sup>-1</sup>. The relaxation experiments were performed on a series of NMR AVANCE spectrometers (Bruker, Ettlingen, Germany) working at a nominal frequency of 500.13, 700.02 and 850.27 MHz. The details of NMR experiments are described in Figures S1 and S2, Supplementary Material.

## 3. Results and Discussion

Using SI-ATRP, the PMA chains were successfully grafted from the surface of initiator immobilized PS NPs prepared by miniemulsion, and resulted in the formation of PS NPs having PMA canopies with different  $\sigma$  and varying  $N$  (Table 1). The increase in size created by the grafting of the PMA canopy resulted in a larger solvodynamic radius ( $R_s$ ) for the samples with longer PMA chains or higher  $\sigma$  (Figure 1b); similar results were also observed in the dry state by TEM measurements (Figure S3, Supplementary Material).

The comparison of the size of the NPs in DCM and in H<sub>2</sub>O by DLS (Figure 1b,c) made it possible to study the swelling of the NPs and the evolution of thickness of the layer of end-grafted polymer chains. The size of the NPs in both DCM and water increased with increasing  $N$  and  $\sigma$ . In addition, DCM is a good solvent for both the PS core and the PMA canopy and both components were swollen in suspension, while water is a poor solvent for both the PS and PMA, and the NPs were in a collapsed state. This variable swelling of the core had a consequence on the apparent  $\sigma$  of the system. In water, because the NP cores were collapsed, the number of chains per unit of surface area was larger than for the same NP in DCM (Table 2).

**Table 1.** Library of PS-PMA core-canopy NPs.

Sample	Grafting Density (Chains nm <sup>-2</sup> )	N	M <sub>n,NMR</sub> (kDa)	M <sub>n,SEC</sub> (kDa)	D	R <sub>s</sub> in DCM (nm)
PS-σ <sub>low</sub>		0				81 ± 20
PS-PMA <sub>3k</sub> -σ <sub>low</sub>		35	3	4	1.8	86 ± 20
PS-PMA <sub>6k</sub> -σ <sub>low</sub>		70	6	8	2.1	85 ± 30
PS-PMA <sub>18k</sub> -σ <sub>low</sub>	0.07 ± 0.01	209	18	19	2.3	90 ± 20
PS-PMA <sub>28k</sub> -σ <sub>low</sub>		325	28	15	2.2	100 ± 30
PS-PMA <sub>41k</sub> -σ <sub>low</sub>		476	41	18	2.7	100 ± 20
PS-PMA <sub>49k</sub> -σ <sub>low</sub>		569	49	34	2.2	110 ± 20
PS-σ <sub>medium</sub>		0				70 ± 20
PS-PMA <sub>3k</sub> -σ <sub>medium</sub>		30	3	4	1.9	90 ± 30
PS-PMA <sub>7k</sub> -σ <sub>medium</sub>		81	7	9	2.6	90 ± 30
PS-PMA <sub>20k</sub> -σ <sub>medium</sub>	0.46 ± 0.02	232	20	20	2.2	120 ± 40
PS-PMA <sub>30k</sub> -σ <sub>medium</sub>		348	30	27	2.1	170 ± 30
PS-PMA <sub>42k</sub> -σ <sub>medium</sub>		488	42	29	2.1	160 ± 30
PS-PMA <sub>51k</sub> -σ <sub>medium</sub>		592	51	35	2.4	180 ± 40
PS-σ <sub>high</sub>		0				90 ± 20
PS-PMA <sub>3k</sub> -σ <sub>high</sub>		35	3	4	1.7	110 ± 50
PS-PMA <sub>10k</sub> -σ <sub>high</sub>		116	10	12	2.1	130 ± 30
PS-PMA <sub>20k</sub> -σ <sub>high</sub>	1.00 ± 0.12	232	20	21	2.1	160 ± 70
PS-PMA <sub>33k</sub> -σ <sub>high</sub>		383	33	27	2.4	190 ± 30
PS-PMA <sub>42k</sub> -σ <sub>high</sub>		488	42	40	2.5	200 ± 60
PS-PMA <sub>55k</sub> -σ <sub>high</sub>		639	55	44	2.0	240 ± 60

**Table 2.** Grafting density and scaling exponent of PS-PMA core-canopy NPs in DCM and H<sub>2</sub>O.

Grafting Density (σ)	Grafting Density in H <sub>2</sub> O (Chains nm <sup>-2</sup> )	Grafting Density in DCM (Chains nm <sup>-2</sup> )	Scaling Exponent in H <sub>2</sub> O	Scaling Exponent in DCM
Low	0.17	0.07	0.27	0.63
Medium	0.80	0.46	0.50	0.88
High	2.50	1.00	0.55	0.91

In DCM,  $R_s$  of bare PS NPs with  $\sigma_{low}$  was 81 nm and the size increased up to 110 nm for NPs functionalized with PMA chains with  $N = 569$  units. For NPs with  $\sigma_{high}$ ,  $R_s$  of bare PS NPs was 90 nm and increased up to 240 nm when PMA chains with  $N = 639$  units were grafted. The variation of the size of the swollen NPs with the increase of  $N$  (Figure 1b,c) follows the scaling relation:

$$R_s - R_{s,0} \propto N^v \quad (1)$$

where  $R_s$  is the thickness of grafted chains,  $N$  is the degree of polymerization,  $v$  is the scaling exponent and  $R_{s,0}$  is the size of the PS core. The scaling factor was shown to change for different grafting regime [14,15,31,32]. Here, at  $\sigma_{low}$  in DCM the scaling factor ( $v = 0.63$ ) was typical of grafted chains in the semi-collapsed chain regime in a good solvent. For the NPs with  $\sigma_{medium}$  and  $\sigma_{high}$ , the scaling exponent of 0.88 and 0.91 were observed, respectively (Table 2), typical of grafted chains in the stretched regime [14,15]. In water, a poor solvent for the PMA canopy, the stretching factor of the canopy with a  $\sigma_{low}$  was 0.27 typical of collapsed chains. The particles prepared at higher  $\sigma_{medium}$  and  $\sigma_{high}$  dispersed in water showed a stretching parameter corresponding to the semi-collapsed regime. The result obtained for the stretching parameter of the grafted chains the PS-PMA NPs was in keeping with the decrease in solvent quality going from DCM to water. In a good solvent, as a consequence of the polymer-solvent enthalpic attraction and the polymer-polymer entropic repulsion, the grafted polymer chains adopt a stretched and extended conformation [33,34] resulting in a large  $v$ . Conversely, in a poor solvent, the favorable polymer-polymer attraction results in the adoption of a collapsed conformation. If the NPs were dispersed in a good solvent at a high enough concentration, the formation of colloidal



gels was observed [18]. However, the NMR experiments were performed below the solution-to-gel transition to study the dynamics of single particles rather than the dynamics of the NPs network.

The NMR relaxation of the NPs suspension was measured at different magnetic fields and different temperatures to understand the local subsegmental chain dynamics in both the PS core and the PMA canopy. Both the spin-lattice relaxation ( $T_1$ ) and spin-spin relaxation ( $T_2$ ) were measured. The relaxation times obtained by NMR spectroscopy are influenced by  $\tau_c$  of the relaxation process and the interactions between the spin under study and their environment. Typically,  $T_2$  is not largely influenced by the magnetic field used and the values of  $T_2$  can be directly correlated to the subsegmental relaxation [35]. As the local mobility of the molecules under investigation decreases, the value of the  $T_2$  time decreases, and for very slow systems, it can be difficult to quantify the  $T_2$  relaxation precisely without using alternative pulse sequences. Consequently, the measurement of the  $T_2$  of the crosslinked PS core was challenging. Thus,  $T_1$  relaxation time, although providing less precise measurement of the local subsegmental chain relaxation, was also used to probe the PS-PMA NPs.

The  $T_2$  of PMA was used to probe the relaxation dynamics of the tethered chains (Figure 2a). The  $T_2$  of free PMA chains depicted ca. 0.77 s at  $N = 46$  and slightly decreased with an increase of  $N$ . The short tethered PMA chains ( $N = 35$ ) at  $\sigma_{\text{low}}$  showed a  $T_2$  of 0.42 s and as chain length increased, the  $T_2$  value also moderately increased. The increase in the  $T_2$  value indicates an enhanced subsegmental mobility of the chains. Thus, it can be concluded that the local mobility of the tethered PMA chains with  $\sigma_{\text{low}}$  increased when the  $N$  of the chain increased. Even though the PMA chains on the PS-PMA NPs at  $\sigma_{\text{low}}$  displayed a collapsed brush conformation, given their chain stretching factor (Table 2), their local subsegmental mobility was reduced in comparison to untethered PMA chains of the same length, likely because the presence of the PS substrate restricted the subsegmental motion of the chains. As  $\sigma$  increased from low to high, the  $T_2$  of the short tethered PMA decreased due to the transition from a collapsed conformation to a stretched brush regime (Table 2) generated by the crowding produced by the adjacent chains. The relaxation of the free and untethered PMA chains was not influenced by the  $N$  in the range of molecular weights studied. However, for the grafted chains, as the chain length increased, the  $T_2$  of the grafted PMA chains systematically increased for all  $\sigma$ . The increase in the local mobility of the grafted PMA chains as  $N$  increased was attributed to the reduction in the spatial crowding observed as the distance from the core increased with increasing  $N$  [13]. These observations are in keeping with what has been observed for the local subsegmental dynamics of polymer chains grafted to the rigid nanoparticles [19,36].

In the PS-PMA NPs system, both the PMA and the PS were undergoing relaxation. Addressing the effect of the grafting of polymer chains on the dynamics of the soft core can be the key to explain the divergences observed when comparing the macroscopic properties of soft and hard polymer-functionalized particles [18]. However, the local dynamics of the crosslinked PS core was too slow to be probed efficiently by the measurement of the  $T_2$  (Figure S4, Supplementary Material). In the slow regime, the  $T_1$  of a proton will increase as the local chain  $\tau_c$  decreases. Furthermore, the  $T_1$  values are significantly influenced by the local magnetic field. Consequently, to get a clear picture of the chain relaxation in the PS cores  $T_1$  relaxation times were measured at different magnetic fields (Figure S5, Supplementary Material).

The relaxation of all the unfunctionalized PS cores exhibited similar  $T_1$  relaxation times. The grafting of PMA chains of different  $N$  at  $\sigma_{\text{low}}$  resulted in no significant changes in the  $T_1$  value observed. However, when PS cores were functionalized with PMA chains at  $\sigma_{\text{medium}}$  and  $\sigma_{\text{high}}$ , the  $T_1$  of the PS core decreased with the increase of  $N_{\text{PMA}}$ . (Figure 2b) Consequently, at  $\sigma_{\text{medium}}$  and  $\sigma_{\text{high}}$  the grafting of the PMA chains increased the mobility of the PS core, and this effect was more pronounced with longer chains.

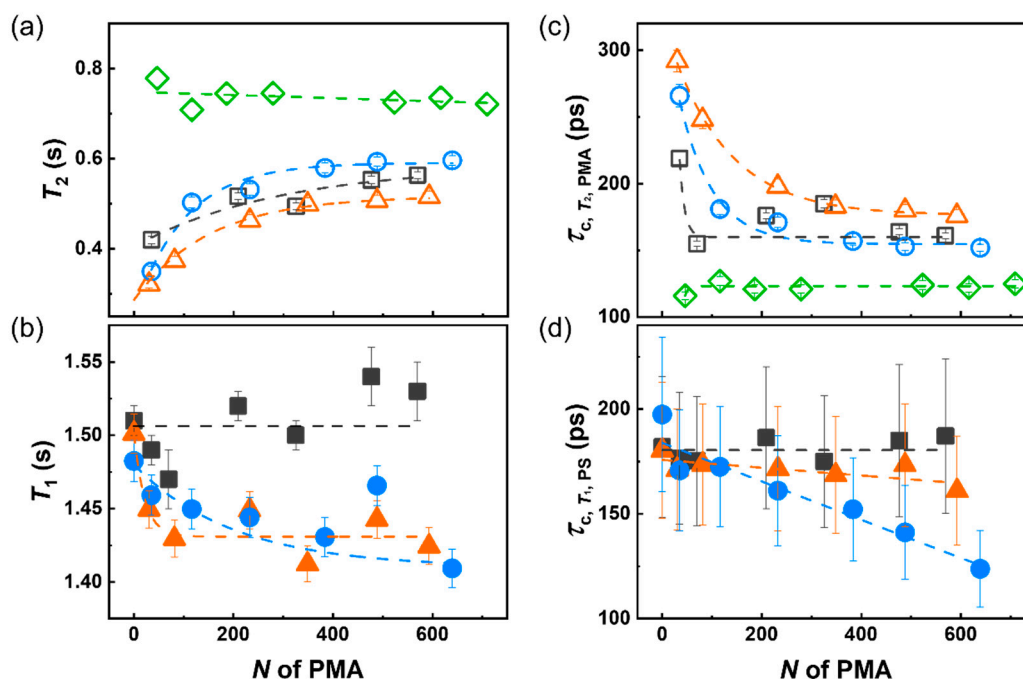


**Figure 2.** (a)  $^1\text{H}$  spin–spin relaxation time of methoxy group of the PMA canopy and (b)  $^1\text{H}$  spin–lattice relaxation time of aromatic ring of the PS core in the PS–PMA NPs with different degrees of polymerization of the PMA chains ( $N$ ) grafted on PS cores with different grafting density, measured at 298 K by using an NMR spectrometer at a Larmor frequency of 700.02 MHz; (c) Correlation time of  $^1\text{H}$  of methoxy group of PMA canopy obtained from  $T_2$  relaxation and (d) correlation time of  $^1\text{H}$  of the aromatic ring of PS core obtained from  $T_1$  relaxation, calculated from BPP theory. For PS–PMA NPs with low (0.17 chains  $\text{nm}^{-2}$ ,  $\square$ ), medium (0.8 chains  $\text{nm}^{-2}$ ,  $\triangle$ ), high (2.5 chains  $\text{nm}^{-2}$ ,  $\circ$ ) grafting density and free PMA chain ( $\diamond$ ).

The relaxation time  $T_1$  and  $T_2$  obtained by NMR spectroscopy are measures of the relaxation of the spins system, an indirect measurement of the local dynamics, those values can be used to calculate the  $\tau_c$  of subsegmental motions of the chains [35]. The average  $\tau_c$  of the PMA chains and of the PS core were independently measured from the  $T_2$  for the PMA and  $T_1$  for the PS. The  $\tau_c$  of free PMA chains was not significantly affected by  $N$  (Figure 2c) in the range of molecular weight studied. The grafting of the PMA chains to the PS core resulted in a decrease of in the local subsegmental mobility of the PMA chains resulting in larger  $\tau_c$  values for the grafted PMA chains in comparison to the free PMA chains. As the  $\sigma$  increased, the constrain on each chain created by the neighboring chains increased and led to the increase in  $\tau_c$  observed especially at low  $N$ . At every  $\sigma$  as  $N$  increased, the difference in  $\tau_c$  of the free and grafted PMA chains decreased. The  $\tau_c$  measured by NMR relaxation is the average  $\tau_c$  for the chains, and the decrease in the average  $\tau_c$  of the PMA chain with increasing  $N$  suggested that the reduced dynamics experienced by the PMA segments was more important close to the interface with the PS core, in keeping with the decrease of monomer concentration as the distance from the surface increases, which reduced the crowding generated by neighboring chains [13]. Furthermore, as the length of the chains increased the difference observed for the nanoparticles with different  $\sigma$  decreased, because the segments of the grafted chains farther away from the core are less constrained at every  $\sigma$ , in keeping with observation of polymer chains grafted to hard nanoparticle cores [16].

Furthermore, the grafting of the PMA chains to the PS core influenced the local dynamics of the PS cores. After the grafting of the PMA chain at the interface of the PS NPs, a limited decrease in the  $\tau_c$  of the PS core was observed, and this effect was stronger when the surface of the PS NPs was functionalized with long PMA chains (Figure 2d). Furthermore, as  $\sigma$  increased, the impact of the PMA chains on the dynamics of the PS core increased. This result can be attributed to an interplay between

the slow dynamics of PS core and faster dynamics of PMA canopy. A similar behavior can be observed for block copolymer when a component with a high relaxation rate, increases the local dynamics of a slower block, because of the increased local fluctuations of the junction between the two segments initiated by the faster component [37,38]. Additionally, the effect of  $\sigma$  suggests that the number of grafted chains, rather than the dynamics of the grafted chains themselves, was the driving force for the faster dynamics observed with the PS core functionalized with a high number of long PMA chains.

The variation of the  $\tau_c$  of a solvated polymer at different temperatures (Figure 3) can be described as an Arrhenius relation, where the activation energy associated with the subsegmental relaxation of the chains (Figure 4a,b) is a measure of the cooperativity of the segmental movement [39–41]. As the temperature increased, the  $\tau_c$  of the PMA chains decreased as expected (Figure 3a,b), since higher temperatures increase the local subsegmental mobility of the polymer. However, in the case of the PS core, the  $\tau_c$  increased with an increase in the temperature (Figure 3c,d). This unexpected result is related to the deswelling of crosslinked PS observed at high temperatures in specific solvent systems (Figure S6 Supplementary Material, ) [12,42].

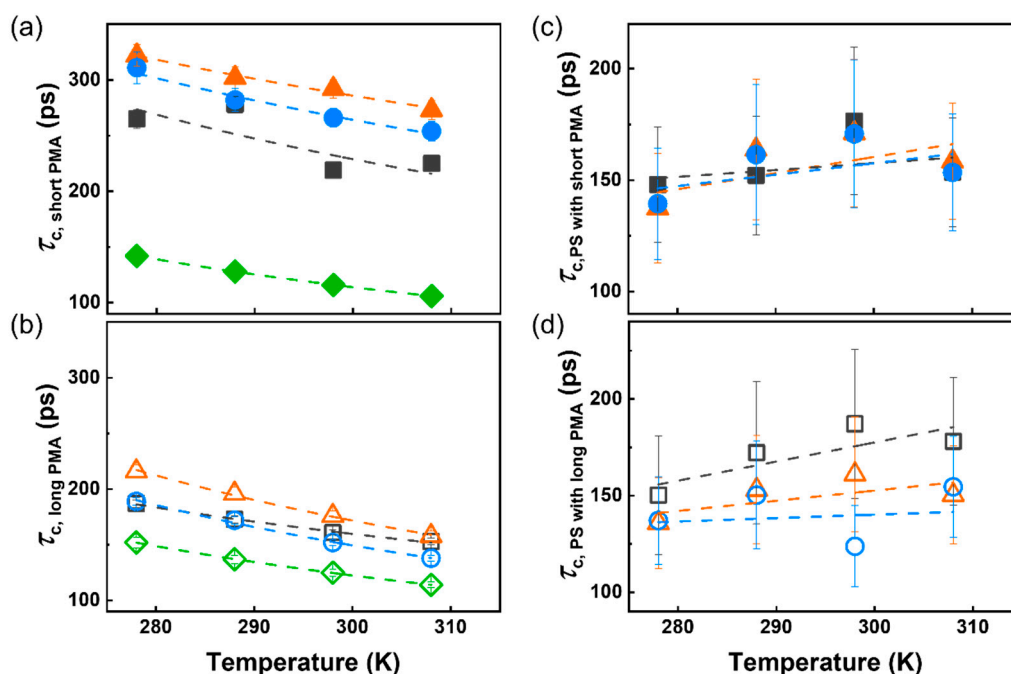


**Figure 3.** Temperature dependence of correlation time of PMA canopy with (a) short chains ( $N < 50$ ), (b) long chains ( $N > 500$ ), PS core with (c) short PMA chains and (d) long PMA chains. For PS-PMA NPs with low ( $0.17 \text{ chains nm}^{-2}$ ,  $\square$ ), medium ( $0.8 \text{ chains nm}^{-2}$ ,  $\triangle$ ), high ( $2.5 \text{ chains nm}^{-2}$ ,  $\circ$ ) grafting density and free PMA chain ( $\diamond$ ).

The energy of activation of the PMA chains of PS-PMA core-canopy NPs was calculated using the  $\tau_c$  measured at different temperatures (Figure 4a). As expected, the activation energy associated with the subsegmental dynamics of the untethered PMA chains did not change significantly with  $N$ . However, short grafted chains displayed lower activation energy than the free chains, indicative of a decrease in the degree of cooperativity associated with the relaxation process, in keeping with the conformational changes of the PMA chains upon grafting when the chains adopted a partially stretched conformation. As the  $N$  increases, the difference in the extent of cooperativity of the relaxation process between the grafted chain and the free chains decreased. As a result of the limited weight fraction of PMA in the PS-PMA samples prepared at a low  $\sigma$ , the measurements were not as precise, and no clear conclusion to the effect of the  $\sigma$  can be drawn. In the case of the PS core, the results are more complex; the deswelling of the PS core led to the reduction in the local subsegmental mobility of the PS core and



resulted in apparent negative activation energy for the relaxation process (Figure S4, Supplementary Material). Nonetheless, the results clearly show that the grafting of the PMA chains facilitated the relaxation of the PS core, and this effect was more pronounced for long chains grafted with  $\sigma_{\text{high}}$  and  $\sigma_{\text{medium}}$  than with  $\sigma_{\text{low}}$ .

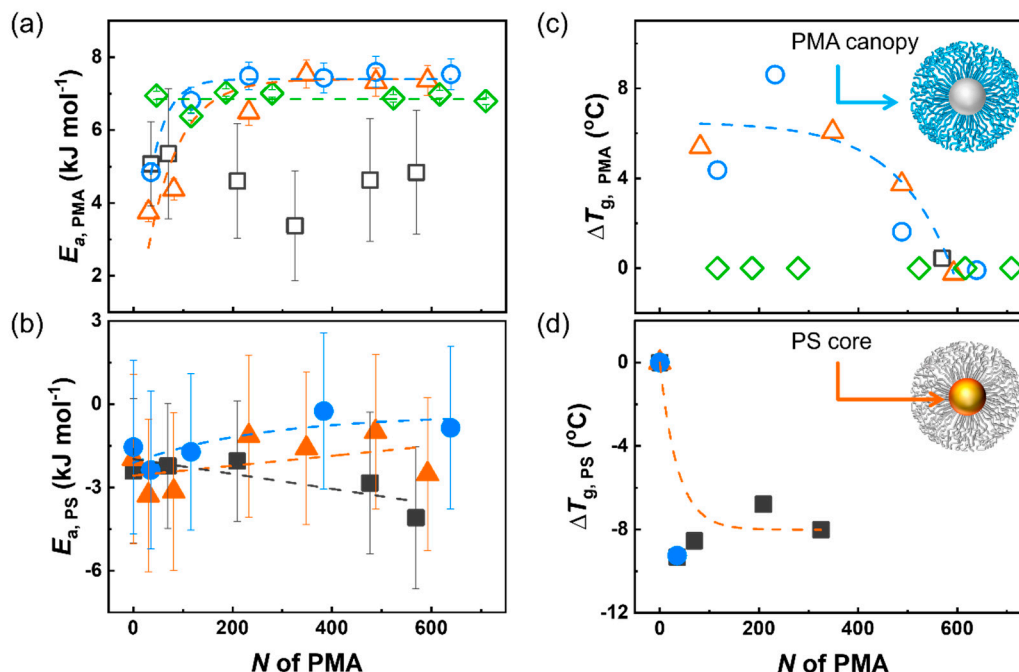


**Figure 4.** Energy of activation of local segmental motion of (a) PMA canopy and (b) PS core in PS-PMA NPs; Glass transition temperature ( $T_g$ ) difference between (c) free PMA and tethered PMA in PS-PMA with different degrees of polymerization of the PMA chains ( $\Delta T_{g,PMA} = T_{g,PMA}$  in PS-PMA  $- T_{g,free}$  PMA) and (d) are PS NPs and PS core of PS-PMA NPs ( $\Delta T_{g,PS} = T_{g,PS}$  in PS-PMA  $- T_{g,bare}$  PS). For PS-PMA NPs with low (0.17 chains  $\text{nm}^{-2}$ ,  $\square$ ), medium (0.8 chains  $\text{nm}^{-2}$ ,  $\triangle$ ), high (2.5 chains  $\text{nm}^{-2}$ ,  $\circ$ ) grafting density and free PMA chain ( $\diamond$ ).

The activation energy measured for the DCM suspensions of the PS-PMA NPs clearly demonstrated an interaction between the dynamics of the PS core and the dynamics of the PMA canopy. Similar trends are also observed in the solid-state. The thermal behavior of dried PS-PMA (Figure 4c,d) showed that both the glass transition temperature of the PS core and of the PMA canopy was affected by the architecture of the PMA canopy. The untethered PMA chains displayed a moderate increase (ca. 2  $^{\circ}\text{C}$ ) of glass transition temperature with the  $N$  as expected from the Flory-Fox equation [43,44]. Short PMA chains grafted to the PS core displayed a glass transition temperature systematically higher than free PMA chains of the same molecular weight. The difference in the glass transition temperature of free and tethered chains decreased with increasing  $N$ . The results observed for the grafted PMA chains were consistent with what has been observed when polymer chains tethered to rigid NP cores transitioned between a highly stretched to a more relaxed brush regime [21,45]. In addition, it was found that the glass transition temperature of PS core (Figure 4b; Table S1, Supplementary Material) significantly decreased by grafting PMA chains to the PS core. The grafting of the PMA chains on the surface of the PS core softened the core, in keeping with the increased local subsegmental mobility observed by NMR relaxation in the swollen nanoparticles suspensions.

#### 4. Conclusions

In conclusion, using NMR relaxation, we showed that the local segmental dynamics of PS-PMA NPs in suspension depends on the architecture of the system. The degree of polymerization and the grafting density influenced the dynamics of the interfacial layer of end-tethered PMA chain,

as observed in other systems where mobile chains were grafted to rigid substrates, but also influenced the dynamics of the PS core. The results presented here also show a unique phenomenon: the grafting of a polymer canopy to a swollen and deformable PS core also influenced the dynamics of the core. The grafting of PMA chain to the PS core facilitated the subsegmental relaxation of the PS network. The fastest local PS dynamics were observed when long chains were densely grafted to the PS core. The cooperative nature of the relaxation decreased for the grafted PMA chains in comparison to the free PMA chains. However, this effect was amplified for short chains, and this can be related to the conformational change in the polymer chains upon grafting. The local subsegmental motion of the PS-PMA NPs in suspensions correlates with the global thermal movement of the system in dry state measured by differential calorimetry.

**Supplementary Materials:** The following are available online at <http://www.mdpi.com/2073-4360/12/8/1844/s1>, Figure S1: Inversion-recovery NMR experiment, Figure S2: CPMG NMR experiment, Figure S3: Solvodynamic size distribution and TEM images of NPs, Figure S4: Temperature dependent  $T_2$  relaxation of PS-PMA NPs, Figure S5: Temperature and magnetic field strength dependent  $T_1$  relaxation of PS-PMA NPs, Figure S6: Temperature dependent swelling of NPs, Table S1: Glass transition temperature of PS and PMA.

**Author Contributions:** Y.-G.K. and H.T.-A. designed the experiments. W.W. synthesized the samples and Y.-G.K. performed the NMR experiments. Y.-G.K. and H.T.-A. analyzed the data and discussed the results. Y.-G.K. and H.T.-A. wrote the manuscript. All authors have read and agreed to the published version of the manuscript.

**Funding:** The authors acknowledge the financial support of the Max Planck Center for Complex Fluid Dynamics.

**Acknowledgments:** The authors thank Katharina Landfester for fruitful discussions and support. The authors are thankful to Manfred Wagner and Petra Kindervater for their help with NMR measurements, as well as to Katrin Kirchoff, Elke Muth and Michael Steiert for TEM, DSC and ICP-AES measurements.

**Conflicts of Interest:** The authors declare no conflict of interest.

## References

1. Srivastava, S.; Agarwal, P.; Archer, L.A. Tethered nanoparticle-polymer composites: Phase stability and curvature. *Langmuir* **2012**, *28*, 6276–6281. [[CrossRef](#)] [[PubMed](#)]
2. Hu, H.; Xiu, K.M.; Xu, S.L.; Yang, W.T.; Xu, F.J. Functionalized layered double hydroxide nanoparticles conjugated with disulfide-linked polycation brushes for advanced gene delivery. *Bioconjugate Chem.* **2013**, *24*, 968–978. [[CrossRef](#)] [[PubMed](#)]
3. Vogiatzis, G.G.; Theodorou, D.N. Structure of polymer layers grafted to nanoparticles in silica-polystyrene nanocomposites. *Macromolecules* **2013**, *46*, 4670–4683. [[CrossRef](#)]
4. Sato, T.; Ohishi, T.; Higaki, Y.; Takahara, A.; Otsuka, H. Radical crossover reactions of alkoxyamine-based dynamic covalent polymer brushes on nanoparticles and the effect on their dispersibility. *Polym. J.* **2016**, *48*, 147–155. [[CrossRef](#)]
5. Zoppe, J.O.; Ataman, N.C.; Mocny, P.; Wang, J.; Moraes, J.; Klok, H.-A. Surface-initiated controlled radical polymerization: State-of-the-art, opportunities, and challenges in surface and interface engineering with polymer brushes. *Chem. Rev.* **2017**, *117*, 1105–1318. [[CrossRef](#)]
6. Schöttler, S.; Becker, G.; Winzen, S.; Steinbach, T.; Mohr, K.; Landfester, K.; Mailänder, V.; Wurm, F.R. Protein adsorption is required for stealth effect of poly(ethylene glycol)- and poly(phosphoester)-coated nanocarriers. *Nat. Nanotechnol.* **2016**, *11*, 372–377. [[CrossRef](#)]
7. Prencipe, G.; Tabakman, S.M.; Welsher, K.; Liu, Z.; Goodwin, A.P.; Zhang, L.; Henry, J.; Dai, H. PEG branched polymer for functionalization of nanomaterials with ultralong blood circulation. *J. Am. Chem. Soc.* **2009**, *131*, 4783–4787. [[CrossRef](#)]
8. Koerner, H.; Drummy, L.F.; Benicewicz, B.; Li, Y.; Vaia, R.A. Nonisotropic self-organization of single-component hairy nanoparticle assemblies. *ACS Macro Lett.* **2013**, *2*, 670–676. [[CrossRef](#)]
9. Dahal, U.; Wang, Z.; Dormidontova, E.E. Hydration of spherical PEO-grafted gold nanoparticles: Curvature and grafting density effect. *Macromolecules* **2018**, *51*, 5950–5961. [[CrossRef](#)]
10. Ethier, J.G.; Hall, L.M. Structure and entanglement network of model polymer-grafted nanoparticle monolayers. *Macromolecules* **2018**, *51*, 9878–9889. [[CrossRef](#)]

11. Sakib, N.; Koh, Y.P.; Huang, Y.; Mongcopa, K.I.S.; Le, A.N.; Benicewicz, B.C.; Krishnamoorti, R.; Simon, S.L. Thermal and rheological analysis of polystyrene-grafted silica nanocomposites. *Macromolecules* **2020**. [[CrossRef](#)]
12. Kim, Y.-G.; Wagner, M.; Thérien-Aubin, H. Dynamics of soft and hairy polymer nanoparticles in a suspension by NMR relaxation. *Macromolecules* **2020**, *53*, 844–851. [[CrossRef](#)] [[PubMed](#)]
13. Daoud, M.; Cotton, J.P. Star shaped polymers: A model for the conformation and its concentration dependence. *J. Phys.* **1982**, *43*, 531–538. [[CrossRef](#)]
14. Ohno, K.; Morinaga, T.; Takeno, S.; Tsujii, Y.; Fukuda, T. Suspensions of silica particles grafted with concentrated polymer brush: Effects of graft chain length on brush layer thickness and colloidal crystallization. *Macromolecules* **2007**, *40*, 9143. [[CrossRef](#)]
15. Dukes, D.; Li, Y.; Lewis, S.; Benicewicz, B.; Schadler, L.; Kumar, S.K. Conformational transitions of spherical polymer brushes: Synthesis, characterization, and theory. *Macromolecules* **2010**, *43*, 1564–1570. [[CrossRef](#)]
16. Kim, S.A.; Mangal, R.; Archer, L.A. Relaxation dynamics of nanoparticle-tethered polymer chains. *Macromolecules* **2015**, *48*, 6280. [[CrossRef](#)]
17. Akcora, P.; Liu, H.; Kumar, S.K.; Moll, J.; Li, Y.; Benicewicz, B.C.; Schadler, L.S.; Acehan, D.; Panagiotopoulos, A.Z.; Pryamitsyn, V.; et al. Anisotropic self-assembly of spherical polymer-grafted nanoparticles. *Nat. Mater.* **2009**, *8*, 354–359. [[CrossRef](#)]
18. Wichaita, W.; Kim, Y.-G.; Tangboriboonrat, P.; Thérien-Aubin, H. Polymer-functionalized polymer nanoparticles and their behaviour in suspensions. *Polym. Chem.* **2020**, *11*, 2119–2128. [[CrossRef](#)]
19. Wei, Y.; Xu, Y.; Faraone, A.; Hore, M.J.A. Local structure and relaxation dynamics in the brush of polymer-grafted silica nanoparticles. *ACS Macro Lett.* **2018**, *7*, 699–704. [[CrossRef](#)]
20. Savin, D.A.; Pyun, J.; Patterson, G.D.; Kowalewski, T.; Matyjaszewski, K. Synthesis and characterization of silica-graft-polystyrene hybrid nanoparticles: Effect of constraint on the glass-transition temperature of spherical polymer brushes. *J. Polym. Sci. Part B Polym. Phys.* **2002**, *40*, 2667–2676. [[CrossRef](#)]
21. Dang, A.; Hui, C.M.; Ferebee, R.; Kubiak, J.; Li, T.; Matyjaszewski, K.; Bockstaller, M.R. Thermal properties of particle brush materials: Effect of polymer graft architecture on the glass transition temperature in polymer-grafted colloidal systems. *Macromol. Symp.* **2013**, *331–332*, 9–16. [[CrossRef](#)]
22. Askar, S.; Li, L.; Torkelson, J.M. Polystyrene-grafted silica nanoparticles: Investigating the molecular weight dependence of glass transition and fragility behavior. *Macromolecules* **2017**, *50*, 1589–1598. [[CrossRef](#)]
23. Holley, D.W.; Ruppel, M.; Mays, J.W.; Urban, V.S.; Baskaran, D. Polystyrene nanoparticles with tunable interfaces and softness. *Polymer* **2014**, *55*, 58–65. [[CrossRef](#)]
24. Arbe, A.; Pomposo, J.A.; Moreno, A.J.; LoVerso, F.; González-Burgos, M.; Asenjo-Sanz, I.; Iturraspe, A.; Radulescu, A.; Ivanova, O.; Colmenero, J. Structure and dynamics of single-chain nano-particles in solution. *Polymer* **2016**, *105*, 532–544. [[CrossRef](#)]
25. Klonos, P.A.; Patelis, N.; Glynos, E.; Sakellariou, G.; Kyritsis, A. Molecular dynamics in polystyrene single-chain nanoparticles. *Macromolecules* **2019**, *52*, 9334–9340. [[CrossRef](#)]
26. Richter, D.; Kruteva, M. Polymer dynamics under confinement. *Soft Matter* **2019**, *15*, 7316–7349. [[CrossRef](#)]
27. Munkhbat, O.; Canakci, M.; Zheng, S.; Hu, W.; Osborne, B.; Bogdanov, A.A.; Thayumanavan, S. 19F MRI of polymer nanogels aided by improved segmental mobility of embedded fluorine moieties. *Biomacromolecules* **2019**, *20*, 790–800. [[CrossRef](#)]
28. Heatley, F. Nuclear magnetic-relaxation of synthetic-polymers in dilute-solution. *Prog. Nucl. Magn. Reson. Spectrosc.* **1979**, *13*, 47–85. [[CrossRef](#)]
29. McCall, D.W. Nuclear magnetic resonance studies of molecular relaxation mechanisms in polymers. *Acc. Chem. Res.* **1971**, *4*, 223–232. [[CrossRef](#)]
30. Graff, R.W.; Wang, X.; Gao, H. Exploring self-condensing vinyl polymerization of inimers in microemulsion to regulate the structures of hyperbranched polymers. *Macromolecules* **2015**, *48*, 2118–2126. [[CrossRef](#)]
31. Hore, M.J.A. Polymers on nanoparticles: Structure & dynamics. *Soft Matter* **2019**, *15*, 1120–1134. [[CrossRef](#)] [[PubMed](#)]
32. Birshtein, T.M.; Zhulina, E.B. Conformations of star-branched macromolecules. *Polymer* **1984**, *25*, 1453–1461. [[CrossRef](#)]
33. Grest, G.S.; Murat, M. Structure of grafted polymeric brushes in solvents of varying quality: A molecular dynamics study. *Macromolecules* **1993**, *26*, 3108–3117. [[CrossRef](#)]

34. Dimitrov, D.I.; Milchev, A.; Binder, K. Polymer brushes in solvents of variable quality: Molecular dynamics simulations using explicit solvent. *J. Chem. Phys.* **2007**, *127*, 084905. [[CrossRef](#)] [[PubMed](#)]
35. Bloembergen, N.; Purcell, E.M.; Pound, R.V. Relaxation effects in nuclear magnetic resonance absorption. *Phys. Rev.* **1948**, *73*, 679–712. [[CrossRef](#)]
36. Holt, A.P.; Bocharova, V.; Cheng, S.; Kisliuk, A.M.; White, B.T.; Saito, T.; Uhrig, D.; Mahalik, J.P.; Kumar, R.; Imel, A.E.; et al. Controlling interfacial dynamics: Covalent bonding versus physical adsorption in polymer nanocomposites. *ACS Nano* **2016**, *10*, 6843–6852. [[CrossRef](#)]
37. Alegria, A.; Lund, R.; Barroso-Bujans, F.; Arbe, A.; Colmenero, J. Component dynamics in nanostructured PI-PDMS diblock copolymers with PI segregated in lamellas, cylinders, and spheres. *Colloid Polym. Sci.* **2014**, *292*, 1863–1876. [[CrossRef](#)]
38. Lund, R.; Willner, L.; Alegria, A.; Colmenero, J.; Richter, D. Self-concentration and interfacial fluctuation effects on the local segmental dynamics of nanostructured diblock copolymer melts. *Macromolecules* **2008**, *41*, 511–514. [[CrossRef](#)]
39. Helfand, E. Dynamics of conformational transitions in polymers. *Science* **1984**, *226*, 647–650. [[CrossRef](#)]
40. Ngai, K.L.; Roland, C.M. Chemical structure and intermolecular cooperativity: Dielectric relaxation results. *Macromolecules* **1993**, *26*, 6824–6830. [[CrossRef](#)]
41. Pethrick, R.A. Molecular-motion of polymers in solution. *Sci. Prog.* **1975**, *62*, 599–631.
42. Erman, B.; Baysal, B.M. Temperature dependence of swelling of polystyrene networks. *Macromolecules* **1985**, *18*, 1696–1700. [[CrossRef](#)]
43. Fox, T.G.; Flory, P.J. Second-order transition temperatures and related properties of polystyrene. I. Influence of molecular weight. *J. Appl. Phys.* **1950**, *21*, 581–591. [[CrossRef](#)]
44. Fox, T.G.; Flory, P.J. The glass temperature and related properties of polystyrene. Influence of molecular weight. *J. Polym. Sci.* **1954**, *14*, 315–319. [[CrossRef](#)]
45. Zuo, B.A.; Zhang, S.S.; Niu, C.; Zhou, H.; Sun, S.Z.; Wang, X.P. Grafting density dominant glass transition of dry polystyrene brushes. *Soft Matter* **2017**, *13*, 2426–2436. [[CrossRef](#)] [[PubMed](#)]



© 2020 by the authors. Licensee MDPI, Basel, Switzerland. This article is an open access article distributed under the terms and conditions of the Creative Commons Attribution (CC BY) license (<http://creativecommons.org/licenses/by/4.0/>).